



This open access document is posted as a preprint in the Beilstein Archives at <https://doi.org/10.3762/bxiv.2020.103.v1> and is considered to be an early communication for feedback before peer review. Before citing this document, please check if a final, peer-reviewed version has been published.

This document is not formatted, has not undergone copyediting or typesetting, and may contain errors, unsubstantiated scientific claims or preliminary data.

Preprint Title SYNTHESIS AND CHARACTERIZATION OF MESOPOROUS ZINC OXIDE NANOPARTICLES

Authors Vaidehi Katoch, Jaskaran Singh, Neeta R. Sharma and Ravinder P. Singh

Publication Date 14 Sep 2020

Article Type Full Research Paper

ORCID® IDs Ravinder P. Singh - <https://orcid.org/0000-0002-6661-6460>

License and Terms: This document is copyright 2020 the Author(s); licensee Beilstein-Institut.

This is an open access publication under the terms of the Creative Commons Attribution License (<https://creativecommons.org/licenses/by/4.0>). Please note that the reuse, redistribution and reproduction in particular requires that the author(s) and source are credited.

The license is subject to the Beilstein Archives terms and conditions: <https://www.beilstein-archives.org/xiv/terms>.

The definitive version of this work can be found at <https://doi.org/10.3762/bxiv.2020.103.v1>

SYNTHESIS AND CHARACTERIZATION OF MESOPOROUS ZINC OXIDE NANOPARTICLES

Vaidehi Katoch¹, Jaskaran Singh¹, Neeta Raj Sharma¹, Ravinder Pal Singh^{2*}

¹Department of Forensic Science School of Bioengineering and Biosciences, Lovely Professional University, Phagwara, Punjab, India

²School of Mechanical Engineering, Lovely Professional University, Phagwara, Punjab, India

*Corresponding email- er.ravinderpalsingh@gmail.com

Abstract

In this investigation, highly crystalline and mesoporous Zinc oxide (ZnO) nanoparticles with the large surface area were synthesized without calcination. Furthermore, the effects of different pH values on structural, physicochemical and textural properties of ZnO nanoparticles were comprehensively investigated. Rietveld refinement implied that the pH variation had significant effects on the crystal structure of ZnO nanoparticles. The phase, molecular and elemental structures confirmed the formation of ZnO as a major phase in all nanopowders. The morphology of ZnO nanoparticles was irregular with an average size of 45 ± 9 nm. Both phase and atomic structures confirmed the polycrystalline arrangement of ZnO nanoparticles. Moreover, isotherms confirmed the mesoporous structure of all ZnO nanoparticles with superior specific surface area and porosity volume. Thus, owing to the concoction of high crystallinity, superior surface area and porosity volume, resultant ZnO nanoparticles can be effectively employed for diverse multifunctional therapeutic applications.

Keywords: Mesoporous; Nanoparticles; Rietveld; Structure; Zinc oxide

1. Introduction

The nanodimensional semiconductor crystals have been extensively investigated in recent years owing to their novel properties, including controllable particle morphology and size, low toxicity and novel electrical and catalytic abilities [1-2]. An array of semiconductor materials such as silicon, germanium, gallium nitride and gallium arsenide etc. have been extensively employed in electronics and textile industry [3], photovoltaic cells [4], antibacterial [5] and cosmetic applications [6]. Among these novel materials, Zinc oxide (ZnO) nanoparticles have been acclaiming wide attention in solar cells, luminescence, electrical devices and chemicals sensors [7]. The number of investigations has reported a variety of ZnO nanostructures such as nanowires and nanorods [8], nanorings [9], nano-loops [10], nano-combs [11], nano-helices [12], nano-bows [13], nanobelts and nanocages [14]. Many synthesis routes including sol-gel [15-22], wet precipitation [23-27], hydrothermal [28-30], chemical vapour deposition [31], and precipitation [32] methods have been reported to prepare the monolithic ZnO nanoparticles. Among these techniques, the hydrothermal route has been a versatile method owing to several advantages including the formation of novel nanohybrid and nanocomposite materials [33], low-temperature synthesis, cost-effective, strong capacity for scale-up [34] and high temperature-sensitive applications could be created [35].

Furthermore, hydrothermal synthesis of ZnO nanoparticles critically depends on varied synthesis parameters such as molar concentration [36,38] and pH value [30] of precursors, hydrothermal temperature [37] and calcination temperature [29] etc. For instance, an increase in molar concentration of precursors increased to both degree of crystallinity and crystal size of ZnO nanoparticles [36]. The homogenous growth of ZnO particles was observed at a threshold pH value [30]. Similarly, the size of ZnO particles increased with increase in hydrothermal temperature [37],

whereas, decreased with precursor concentration [38]. Furthermore, calcination temperature removed the organic compounds, thus produced the pure crystalline structure of ZnO nanoparticles [29].

Baruah et al. [39] investigated the influence of pH variation on the dimensions and morphology of ZnO nanoparticles prepared using hydrothermal process. The investigation reported that the growth of ZnO nanorods-like particles was rapid in alkaline conditions, whereas, growth of ZnO particles eroded in acidic conditions [39]. Similarly, calcination temperature had a significant effect on the morphology of ZnO nanoparticles. Kumar et al. [40] reported that the morphology and size of ZnO nanoparticles transformed from rods-like to short prisms-like with the increase in the calcination temperature. Wang et al. [41] reported that the ageing temperature had a critical effect on the morphology of ZnO nanoparticles, and the different particle morphologies exhibited different electrical conductivity. Koutu et al. [2] investigated the effects of varying molar concentrations (0.1- 0.4 M) of NaOH precursor on the properties of resultant ZnO nanoparticles. Results revealed that the diameter of ZnO nanoparticles decreased with the increase in molar concentration of NaOH. Therefore, a comprehensive literature review suggested significant effects of varied synthesis parameters on structural and physicochemical properties of ZnO nanoparticles. Apart from it, few reports have been available which have investigated the textural properties of ZnO nanoparticles.

Herein, with this motivation, ZnO nanoparticles were hydrothermally synthesized using solid solutions with different pH values. The structural, physicochemical and textural properties of nanoparticles were comprehensively studied using XRD, FTIR, FESEM, HRTEM, EDX, and BET techniques. The crystal structure of nanoparticles was determined using Rietveld refinement.

The structure-property correlations were comprehensively discussed in the light of published results.

2. Materials and method

High purity (99%) chemical reagents were employed without further purification. Zinc nitrate hexahydrate (ZNH, Merck) and sodium hydroxide (SH, Merck) were used. The hydrothermal assisted wet precipitation route was employed for synthesis purposes. ZNH was used as Zn^{2+} ion source, and SH was used to control the pH value of the precursor. The synthesis methodology has been schematically shown in Fig 1. Typically, 1 M hydrous precursors of ZNH and SH were separately prepared at room temperature ($27^{\circ}C$). Later, SH precursor was drop-wise added into ZNH precursor under vigorous stirring. The pH value of the solid solution was continuously monitored using a calibrated digital pH meter. The five solid solutions of Zn^{2+} ions were separately prepared with different pH values. After homogeneous mixing, the milky-white suspension was put in Teflon bottle, sealed in a metallic autoclave and heated at $110 \pm 3^{\circ}C$ in an electric furnace for 24 hours. Upon annealing, the resulting crystals were repeatedly centrifuged and washed with distilled water for five times. Later, the obtained products were dried at $100 \pm 3^{\circ}C$ for 24 hours in an air oven and then grounded into a fine powder. The nomenclatures of synthesized products categorized based on the pH value of their solid solutions have been given in Table 1.

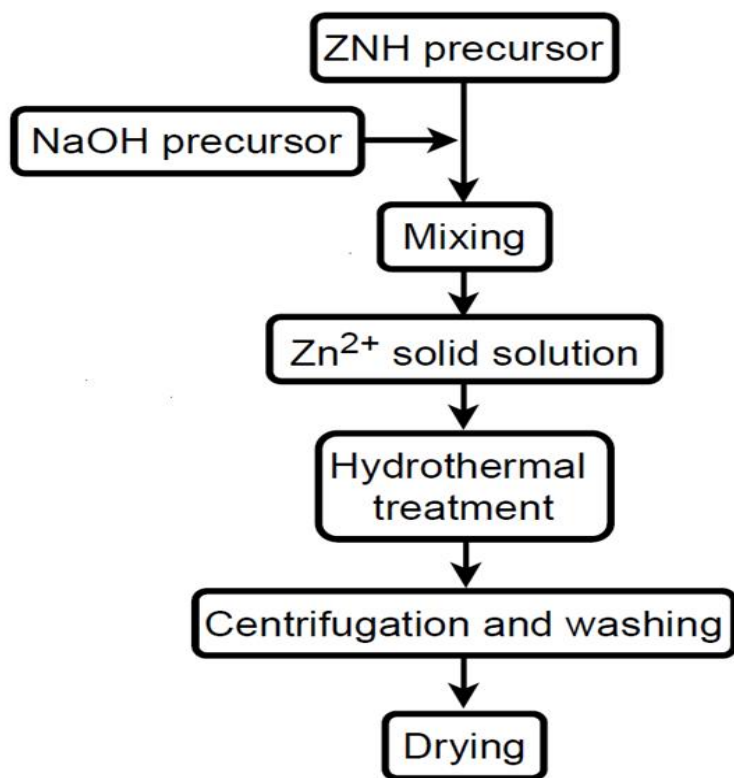


Fig 1: Synthesis methodology

Table 1: The pH value of solid solutions and corresponding nomenclature of synthesized nanopowders

pH value	Nomenclature
7	ZnO7
8	ZnO8
9	ZnO9
10	ZnO10
12	ZnO12

2.1. Characterization

The XRD patterns were obtained using Bruker D8 (Cuk α radiations, $\lambda = 1.54 \text{ \AA}$) from 20° - 70° . For Rietveld refinement, MAUD 2.7 program was used. The XRD patterns were fitted using the polynomial function of the fifth-order and Pseudo-Voigt algorithm. The JCPDS patterns, i.e., 005-0664 for ZnO, 024-1460 for Zinc nitrate hydroxide hydrate (ZNHH), and 025-1028 for Zinc nitrate hydroxide (ZNH) phases, were used.

The crystallite size (X_s) was estimated using the Debye Scherrer formula (Eq. 1):

$$X_s = \frac{0.9 \lambda}{\beta \cos \theta} \quad \text{Eq. (1)}$$

Where λ is the wavelength of radiations, β is full width at half maximum (FWHM), and θ is the diffraction angle. In order to determine the size of ZnO crystals, atomic planes (100), (021), (002), (101), (102), and (110) were considered. Also, Williamson Hall-ISM (Eq. 2) model was used to confirm the crystal size and lattice strain in ZnO crystals. The degree of crystallinity (X_c) was calculated using the peak-area method.

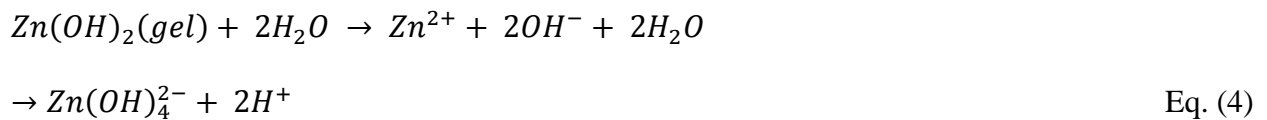
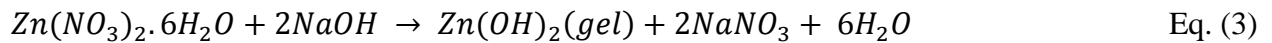
$$\beta_{hkl} \cos(\theta_{hkl}) = \frac{0.9\lambda}{X_s} + 4\varepsilon \sin(\theta_{hkl}) \quad \text{Eq. (2)}$$

Where ε is the lattice strain in ZnO crystals. The Bruker Tensor 27 spectrometer was used to record the FTIR spectra using KBr pellets. The morphology and atomic structure of nanoparticles were studied using FESEM (JEOL JSM-7610F Plus) and HRTEM (FEI Tecnai) electron microscope. The Image-J program was used to measure the dimensions of nanoparticles. The elemental composition of nanoparticles was ascertained using Bruker XFlash 4010 EDX tool. The Autosorb-1-C Quantachrome was employed to measure the specific surface area and porosity of nanoparticles.

3. Results and discussion

3.1. Phase structure

XRD pattern of all nanopowders has been shown in Fig 2. Rietveld refinement suggested biphasic structure (ZnO and ZNH phases) of ZnO7, ZnO8, ZnO9, and ZnO10 nanopowders, whereas, ZnO12 nanopowder was triphasic (ZnO, ZNH and ZNHH) in composition. The ZnO was a principal phase with ZNH and ZNHH were secondary impurities. The characteristic peaks of ZnO, i.e. (100), (002), (101), (102), (110), and (103) were present in all nanopowders as shown in Fig 2. The diffraction peaks of ZnO phase belonged to the hexagonal wurtzite structure [44-46]. Similar diffraction peaks had also been reported in the previous studies [47-49]. It had been speculated that ZNH and ZNHH impurities came from initial ZNH precursor and could not escape from the resultant crystals during centrifugation and washing process. On the other hand, the characteristic peaks of the ZnO phase were distinct, narrow and sharp, which suggested their crystalline structure. Comparison of FWHM values corresponding to (002) and (101) characteristic peaks of ZnO phase (Table 2) indicated that size of ZnO crystals increased with the increase in pH value of ZnO solid solution up to 10. At a pH value of 12, FWHM increased, thereby, indicating the decrease in ZnO crystal size. Thus, the critical analysis implied that the pH variation within 7 to 10 did not transform the phase structure, but affected the size of ZnO crystals. Thus, with the increase in pH value of the ZnO solid solution, resultant ZnO crystals grew. The speculated chemical reaction supporting the formation of ZnO phase has been given in Eq. (3-5) [50].



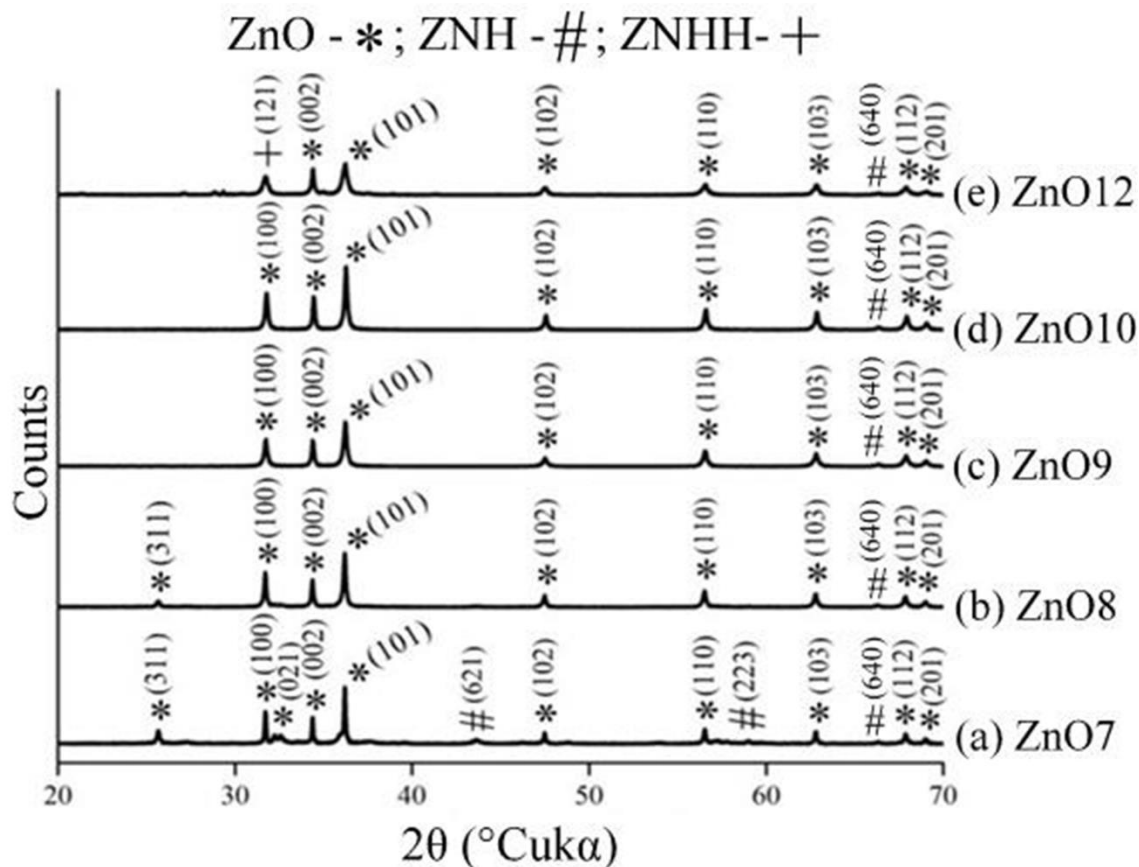


Fig 2: XRD patterns of (a) ZnO7, (b) ZnO8, (c) ZnO9, (d) ZnO10, and (e) ZnO12 nanopowders

Table 2: FWHM values corresponding to (002) and (101) diffraction peaks of ZnO phase pertinent to each nanopowder

Nanopowder	FWHM	
	(002)	(101)
ZnO7	0.1076	0.1135
ZnO8	0.0689	0.1082
ZnO9	0.0492	0.1082
ZnO10	0.0492	0.1079
ZnO12	0.0787	0.2952

3.2. Crystal structure

The fitted XRD profiles obtained after Rietveld refinement have been shown in Fig 3. The goodness of fit parameters (σ , R_{wp} , R_b) and crystal structure parameters of each nanopowder has been given in Table 3. The value of σ for all nanopowders was significantly less than four and was acceptable [51]. With the increase in pH value from 7 to 10, the concentration of stoichiometric ZnO phase increased, whereas, the concentration of ZNH phase decreased. It had been clear that the pH values of nine and 10 were optimal to produce the maximum concentration of ZnO crystals. Although some disparity in the standard ($a= 3.250 \text{ \AA}$ and $c= 5.206 \text{ \AA}$) and experimental lattice parameters of ZnO crystals were observed, interestingly, the distortion ratio (c/a) of experimental lattice parameters was close to the standard value of 1.60. The ZnO9 nanopowder exhibited stoichiometric lattice parameters of $a= 3.250 \text{ \AA}$ and $c= 5.206 \text{ \AA}$, as mentioned in Table 3. The size of ZnO crystals increased with the increase in pH value up to 10 as calculated using various models (Table 3). Apart from it, all models confirmed the nanodimensional regime of ZnO crystals. The growth pattern of ZnO crystals, as suggested by various crystallographic models (Rietveld, Scherrer, and WH-ISM) agreed with the change in crystal size, as suggested by FWHM interpretation. The ZnO crystals in all nanopowders were subjected to tensile strain. Furthermore, the degree of crystallinity increased with the increase in pH value up to 10, as given in Table 3. The ZnO9 and ZnO10 nanopowders exhibited maximum crystallinity of 98%. Thus, the overall analysis concluded that variation in pH value had a significant influence on the crystal structure of ZnO crystals. The solid solution of nine pH value produced a maximum concentration of ZnO crystals with stoichiometric lattice parameters, nanodimensional size and maximum crystallinity.

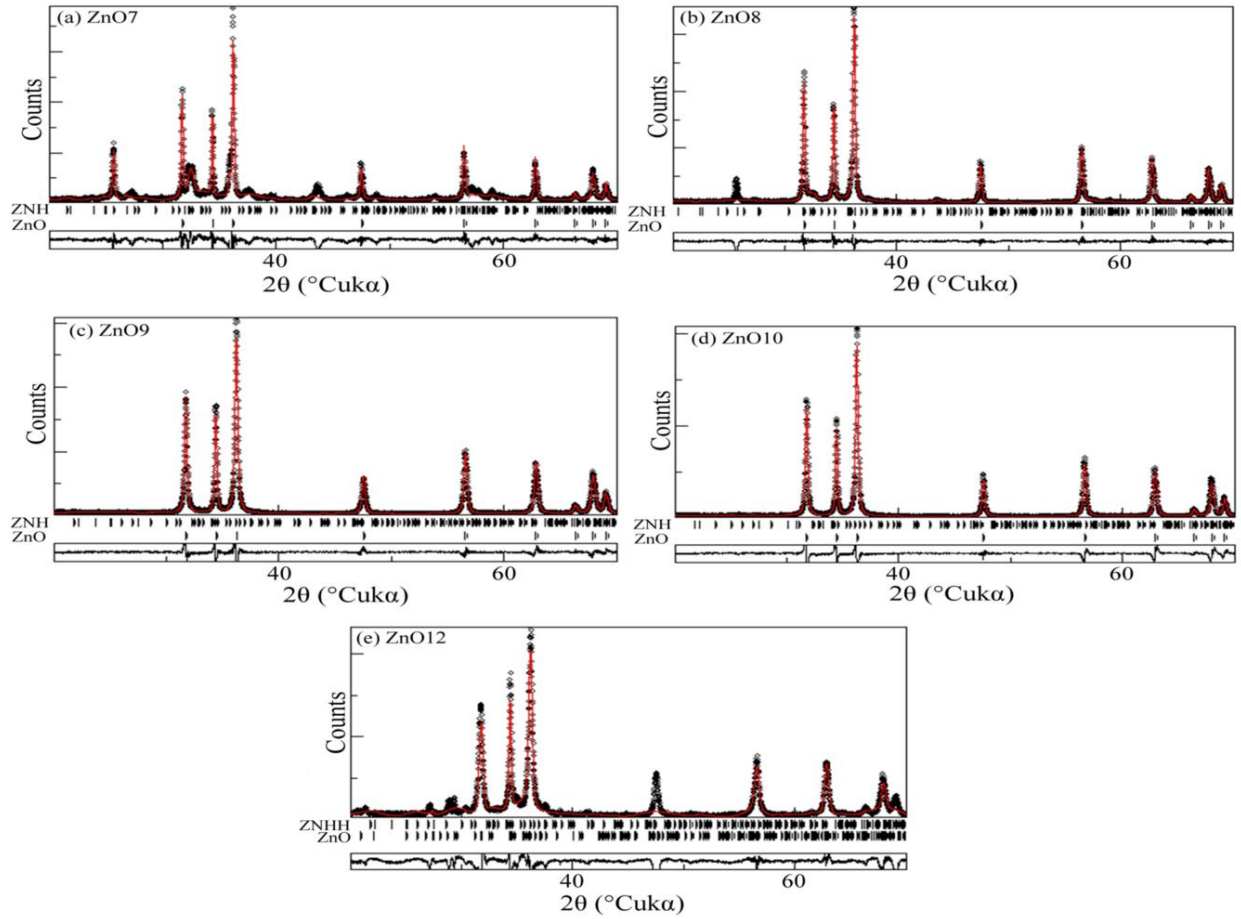


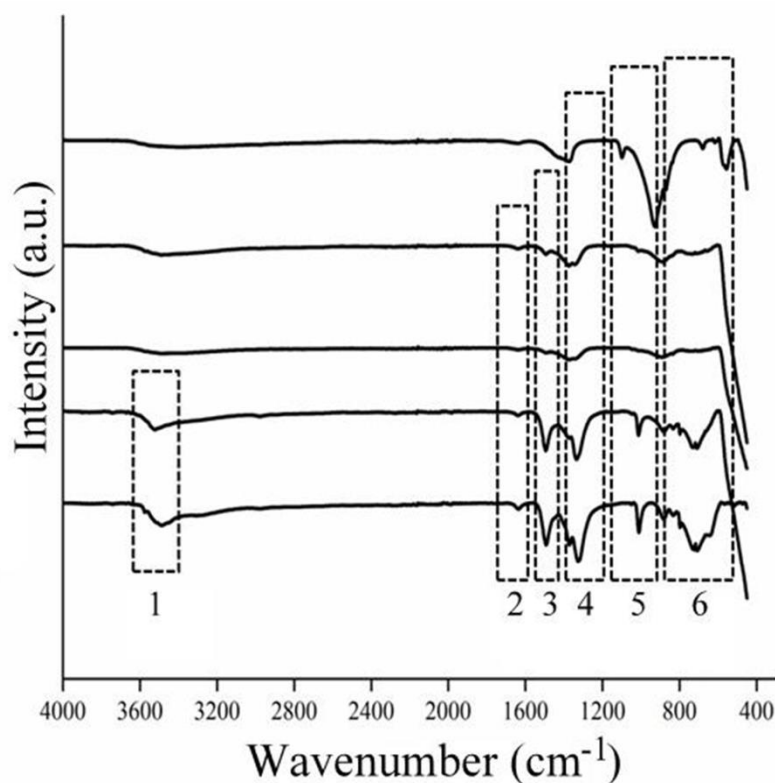
Fig 3: XRD fitted profiles of (a) ZnO7, (b) ZnO8, (c) ZnO9, (d) ZnO10, and (e) ZnO12 nanopowders

Table 3: The goodness of fit values, weight fractions, lattice parameters, crystal size, lattice strain and crystallinity of ZnO crystals pertinent to ZnO7, ZnO8, ZnO9, ZnO10, and ZnO12 nanopowders

NP	Goodness of fit parameters			Weight%			Lattice parameter (Å)		Crystal size (nm)			Microstrain		Crystallinity (%)
	σ	R _{wp}	R _b	ZnO	ZNH	ZNHH	a	c	Rietveld	Scherrer	H-ISM	Rietveld	WH-ISM	
ZnO7	2.098	0.259	0.187	62	38	-	3.252	5.209	12	23± 5	29	0.0002459	0.0006765	88
ZnO8	1.701	0.156	0.093	82	18	-	3.253	5.209	36	42± 6	39	0.0003462	0.0007739	94
ZnO9	1.396	0.136	0.104	98	2	-	3.250	5.206	40	43± 4	52	0.0002788	0.0001148	98
ZnO10	2.050	0.183	0.149	98	2	-	3.248	5.201	48	51± 4	58	0.0002084	0.0001975	98
ZnO12	3.071	0.272	0.201	92	2	6	3.251	5.277	32	41± 3	40	0.0002629	0.0001999	91

3.3. Molecular structure

The FTIR spectra of all nanopowders have been shown in Fig 4. The peaks observed below 500 cm^{-1} and at 1558 cm^{-1} confirmed the formation of Zn-O molecules. In addition to Zn-O ions, vibrations at 910 cm^{-1} and 1020 cm^{-1} suggested the presence of C-O and C-H bonded ions. Furthermore, asymmetric vibrations at 1490 cm^{-1} , 1550 cm^{-1} , and 1640 cm^{-1} were attributed to carboxylic acid (C=O) ions. Carbon had been speculated to come from the atmosphere and entrapped in ZnO crystal structure during stirring and ageing process. In-addition, surface adsorbed water (O-H ions) at 3500 cm^{-1} were also present in all nanopowders. These OH⁻ ions remained entrapped in the surface of as-synthesized nanoparticles and would have been removed upon sintering at high temperature. The following frequencies for metal oxides are also measured by literature values for the respective metal oxides [50-54]. Thus, both phase and molecular structures revealed by XRD and FTIR analysis corroborated formation of ZnO crystals in all nanopowders along with some allied impurities.



S. No.	Wavenumber (cm ⁻¹)	Functional group
1	3500	O-H
2	1640	-C=O
3	1558	Zn-O
4	1490, 1550	Asymmetric vibration of C=O
5	910, 1020	C-O and C-H bond
6	400-800	ZnO- stretching and deformation vibration

Fig 4: FTIR spectra of (a) ZnO7, (b) ZnO8, (c) ZnO9, (d) ZnO10, and (e) ZnO12 nanopowders

3.4. Morphological and elemental structure

The FESEM micrograph of ZnO9 nanoparticles has been shown in Fig 5(a). Particles were irregular in shape and agglomerated. Particles of vivid shapes and size were present in ZnO9 nanopowder. Bigger particles were an agglomeration of numerous smaller particles. Agglomeration of nanoparticles has been a common feature owing to their high surface energy. The average size of individual nanoparticles was 45 ± 9 nm, which was in agreement with the crystal sizes calculated using different models as given in Table 3.

The EDX micrograph of ZnO9 nanoparticles has been shown in Fig 5(b). Presence of Zn and O elements confirmed the formation of ZnO composition. No other element like N and C were detected, whereas, these had been observed in phase and molecular structures, as shown in Fig 2(c) and Fig 4(c), respectively. Elements in traces sometimes could not be detected in EDX analysis. The weight and atomic concentrations of Zn and O elements have been given in Fig 5(b). The weight and atomic ratio of Zn:O were 4.69 and 1.14, respectively, which had been in agreement with the similar results reported elsewhere [55-56].

The HRTEM micrographs showing particle morphology and atomic structure of ZnO9 nanoparticles have been shown in Fig 5(c-d). Particles were confirmed to be irregular in shape and agglomerated [57]. The average size of particles was 47 ± 9 nm. Furthermore, the SAED pattern (Fig 5d) also supported the polycrystalline structure of ZnO crystals in agreement with the XRD phase analysis (Fig 2) [58]. The hexagonal pattern of spots indicated the highly crystalline composition of the particles.

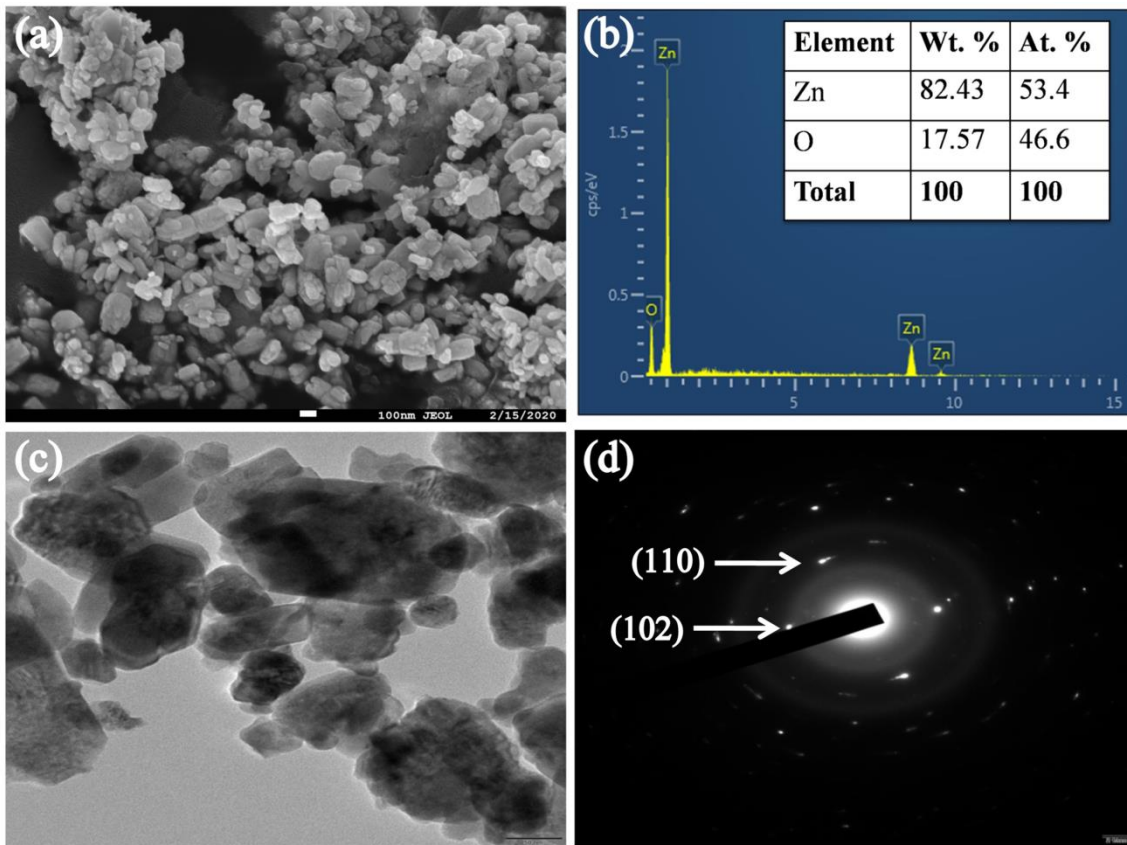


Fig 5: (a) FESEM, (b) EDX, and (c-d) HRTEM micrographs of ZnO9 nanoparticles

3.5. Mesoporous structure

The isotherms and pore size distribution curves (inset) of all nanopowders have been shown in Fig 6. The isotherms of all nanopowders were of type IV with H3 hysteresis loop, suggested the mesoporous structure of nanomaterials. Furthermore, isotherms depicted that the gas adsorption capacity of nanoparticles in increasing order was ZnO10 < ZnO12 < ZnO9 < ZnO8 < ZnO7. Moreover, the BJH curves (inset) suggested the range of diameter of pores between 5- 40 nm, which further confirmed the mesoporous structure of all nanoparticles. The average values of specific surface area and pore volume of nanoparticles have been given in Table 4. Except for ZnO12, the specific surface area of nanoparticles in increasing order was ZnO10 < ZnO9 < ZnO8 < ZnO7. It had already been attributed to the fact that the smaller the particle size (Table 3), greater is their surface area. Interestingly, the surface area of synthesized

nanoparticles was greater than the results reported elsewhere [57-59]. Notably, particles with large particle surface area and porosity volume favour the drug delivery and other similar therapeutic applications requiring superior adsorption capacity.

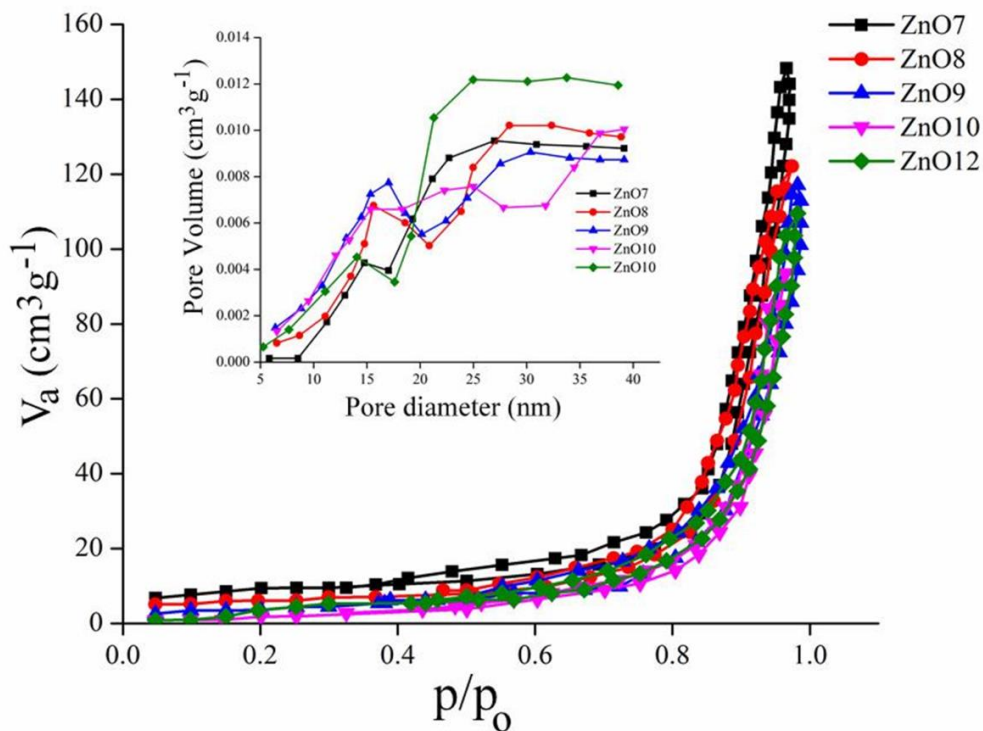


Fig 6: N_2 isotherms and BJH curves (inset) of (a) ZnO7, (b) ZnO8, (c) ZnO9, (d) ZnO10, and (e) ZnO12 nanopowders

Table 4: Specific surface area and pore volume of nanopowders

Nanopowder	BET	BJH
	Specific surface area ($\text{m}^2 \text{g}^{-1}$)	Pore volume ($\text{cm}^3 \text{g}^{-1}$)
ZnO7	62	0.0092
ZnO8	54	0.0095
ZnO9	41	0.0090
ZnO10	30	0.0086
ZnO12	56	0.0106

4. Conclusion

The ZnO nanoparticles were successfully derived from ZnO solid solutions with different pH values. A facile hydrothermal route was employed to prepare the ZnO nanoparticles. The pH variation had little effect on phase and molecular structures of ZnO nanoparticles. On the other hand, pH variation had a significant effect on crystal structure parameters like weight fraction of constituent phases, lattice parameters, crystal size, lattice strain and crystallinity of ZnO nanoparticles. Results implied that the pH value of nine produced the highest concentration of ZnO phase with stoichiometric lattice parameters, nanodimensional crystal size and highest crystallinity. Moreover, ZnO nanoparticles were irregular in shape with an average size of 45 ± 9 nm. The particle sizes calculated using Rietveld, Scherrer, WH-ISM, FESEM and HRTEM models were close to each other. All nanoparticles exhibited a mesoporous structure with superior surface area and porosity. The variation of pH had a significant effect on particle size, and therefore, particle surface area attribute was also dependent on their pH condition during synthesis. Interestingly, the particle surface area of synthesized nanoparticles was superior to the results reported in the literature. Thus, due to the amalgamation of high crystallinity, mesoporous structure, and large particle surface area, the resultant nanoparticles can be employed for several multifunctional therapeutic applications, including drug delivery agents.

Disclosure statement: There is no conflict of interest related to the present work.

Funding information: This research did not receive any specific grant from funding agencies in the public, commercial, or not-for-profit sectors.

References

- [1] Lanje, A. S.; Sharma, S. J.; Ningthoujam, R. S.; Ahn, J. S.; Pode, R. B. Low temperature dielectric studies of zinc oxide (ZnO) nanoparticles prepared by precipitation method. *Advanced Powder Technology*. **2013**, 24(1), 331-335.
- [2] Koutu, V.; Shastri, L.; Malik, M. M. Effect of NaOH concentration on optical properties of zinc oxide nanoparticles. *Materials Science-Poland*. **2016**, 34(4), 819-827.
- [3] Willander, M.; Nur, O.; Sadaf, J. R.; Qadir, M. I.; Zaman, S.; Zainelabdin, A.; Hussain, I. Luminescence from zinc oxide nanostructures and polymers and their hybrid devices. *Materials*. **2010**, 3(4), 2643-2667.
- [4] Umar, A.; Hahn, Y. B. (Eds.). Metal oxide nanostructures and their applications. **2010**, (Vol. 3). American Scientific Publications.
- [5] Podporska-Carroll, J.; Myles, A.; Quilty, B.; McCormack, D. E.; Fagan, R.; Hinder, S. J.; Pillai, S. C. Antibacterial properties of F-doped ZnO visible light photocatalyst. *Journal of Hazardous Materials*. **2017**, 324, 39-47.
- [6] Masaki, T.; Kim, S. Synthesis of nano-sized ZnO powders prepared by precursor process. *Journal of Ceramic Processing & Research*. **2003**, 4(3), 135-139.
- [7] Guo, L.; Yang, S.; Yang, C.; Yu, P.; Wang, J.; Ge, W.; Wong, G. K. Highly monodisperse polymer-capped ZnO nanoparticles: preparation and optical properties. *Applied Physics Letters*. **2000**, 76(20), 2901-2903.
- [8] Baruah, S.; Thanachayanont, C.; Dutta, J. Growth of ZnO nanowires on nonwoven polyethylene fibers. *Science and Technology of Advanced Materials*. **2008**, 9(2), 025009.
- [9] Huang, Y.; Zhang, Y.; Bai, X.; He, J.; Liu, J.; Zhang, X. Bicrystalline zinc oxide nanocombs. *Journal of Nanoscience and Nanotechnology*. **2006**, 6(8), 2566-2570.
- [10] Hughes, W. L.; Wang, Z. L. Controlled synthesis and manipulation of ZnO nanorings and nanobows. *Applied Physics Letters*. **2005**, 86(4), 043106.

- [11] Kong, X. Y.; Wang, Z. L. Spontaneous polarization-induced nanohelices, nanosprings, and nanorings of piezoelectric nanobelts. *Nano Letters*. **2003**, (12), 1625-1631.
- [12] Hughes, W. L.; Wang, Z. Formation of piezoelectric single-crystal nanorings and nanobows. *Journal of the American Chemical Society*. **2004**, 126(21), 6703-6709.
- [13] Sun, T., Qiu, J.; Liang, C. Controllable fabrication and photocatalytic activity of ZnO nanobelt arrays. *The Journal of Physical Chemistry C*. **2008**, 112(3), 715-721.
- [14] Snure, M.; Tiwari, A. Synthesis, characterization, and green luminescence in ZnO nanocages. *Journal of Nanoscience and Nanotechnology*. **2007**, 7(2), 481-485.
- [15] Ranvir S. P.; Preparation of modified ZnO nanoparticles by sol-gel process and their characterization, Master of Technology, **2009**, Thapar University, Punjab.
- [16] Huang, X. H.; Guo, R. Q.; Wu, J. B.; Zhang, P. Mesoporous ZnO nanosheets for lithium ion batteries. *Materials Letters*. **2014**, 122, 82-85.
- [17] Li, L. H.; Deng, J. C.; Deng, H. R.; Liu, Z. L.; Xin, L. Synthesis and characterization of chitosan/ZnO nanoparticle composite membranes. *Carbohydrate Research*. **2010**, 345(8), 994-998.
- [18] Boundifa, A.; Zhang, C.; Lahem, M. Highly sensitive and rapid NO₂ gas sensors based on ZnO nanostructures and the morphology effect on their sensing performances. **2012**, In the 14th International Meeting on Chemical Sensor (IMCS).
- [19] Kolekar, T. V.; Yadav, H. M.; Bandgar, S. S.; Deshmukh, P. Y. Synthesis by sol-gel method and characterization of ZnO nanoparticles. *Indian Streams Research Journal*. **2011**, 1(1), 1-4.
- [20] Zak, A. K.; Razali, R.; Majid, W. A.; Darroudi, M. Synthesis and characterization of a narrow size distribution of zinc oxide nanoparticles. *International Journal of Nanomedicine*. **2011**, 6, 1399.

- [21] Surye P.G. (2012). Synthesis and characterization of zinc oxide nanoparticles by sol-gel process, Master of Science in Physics, National Institute of Technology Rourkela, Orissa, India, 1-36.
- [22] Dutta, S.; Ganguly, B. N. Characterization of ZnO nanoparticles grown in presence of Folic acid template. *Journal of Nanobiotechnology*. **2012**, 10(1), 29.
- [23] Xu, S.; Wang, Z. L. One-dimensional ZnO nanostructures: solution growth and functional properties. *Nano Research*.**2011**, 4(11), 1013-1098.
- [24] Kołodziejczak-Radzimska, A.; Jesionowski, T. Zinc oxide- from synthesis to application: a review. *Materials*. **2014**, 7(4), 2833-2881.
- [25] Samanta, P. K.; Patra, S. K.; Ghosh, A.; Chaudhuri, P. R. Visible emission from ZnO nanorods synthesized by a simple wet chemical method. *International Journal of Nanoscience and Nanotechnology*. **2009**, 1(1-2), 81-90.
- [26] Bindu, P.; Thomas, S. Estimation of lattice strain in ZnO nanoparticles: X-ray peak profile analysis. *Journal of Theoretical and Applied Physics*. **2014**, 8(4), 123-134.
- [27] Wahid, K. A.; Lee, W. Y.; Lee, H. W.; Teh, A. S.; Bien, D. C.; Azid, I. A. Effect of seed annealing temperature and growth duration on hydrothermal ZnO nanorod structures and their electrical characteristics. *Applied Surface Science*.**2013**, 283, 629-635.
- [28] Madathil, A. N. P.; Vanaja, K. A.; Jayaraj, M. K. Synthesis of ZnO nanoparticles by hydrothermal method. *Nanophotonic Materials IV* **2007**, (Vol. 6639, p. 66390J). International Society for Optics and Photonics.
- [29] Cheng, B.; Samulski, E. T. Hydrothermal synthesis of one-dimensional ZnO nanostructures with different aspect ratios. *Chemical Communications*. **2004**, (8), 986-987.
- [30] Rouhi, J.; Alimanesh, M.; Mahmud, S.; Dalvand, R. A.; Ooi, C. R.; Rusop, M. A novel method for synthesis of well-aligned hexagonal cone-shaped ZnO nanostructures in field emission applications. *Materials Letters*. **2014**, 125, 147-150.

- [31] Macias-Martinez, B. I.; Cortes-Hernandez, D. A.; Zugasti-Cruz, A.; Cruz-Ortíz, B. R.; Múzquiz-Ramos, E. M. Heating ability and hemolysis test of magnetite nanoparticles obtained by a simple co-precipitation method. *Journal of Applied Research and Technology*. **2016**, 14(4), 239-244.
- [32] Shinde, S. D.; Patil, G. E.; Kajale, D. D.; Ahire, D. V.; Gaikwad, V. B.; Jain, G. H. Synthesis of ZnO nanorods by hydrothermal method for gas sensor applications. *International Journal on Smart Sensing & Intelligent Systems*. **2012**, 5(1).
- [33] Li, X.; Zhang, F.; Ma, C.; Deng, Y.; Wang, Z.; Elingarami, S.; He, N. Controllable synthesis of ZnO with various morphologies by hydrothermal method. *Journal of Nanoscience and Nanotechnology*. **2012**, 12(3), 2028-2036.
- [34] Bai, S. N.; Wu, S. C. Synthesis of ZnO nanowires by the hydrothermal method, using sol-gel prepared ZnO seed films. *Journal of Materials Science: Materials in Electronics*. **2011**, 22(4), 339-344.
- [35] Moazzen, M. A. M.; Borghei, S. M.; Taleshi, F. Change in the morphology of ZnO nanoparticles upon changing the reactant concentration. *Applied Nanoscience*. **2013**, 3(4), 295-302.
- [36] Ridhuan, N. S.; Razak, K. A.; Lockman, Z.; Aziz, A. A. Structural and morphology of ZnO nanorods synthesized using ZnO seeded growth hydrothermal method and its properties as UV sensing. *PloS one*. **2012**, 7(11).
- [37] Mahmood, M. A.; Jan, S.; Shah, I. A.; Khan, I. Growth parameters for films of hydrothermally synthesized one-dimensional nanocrystals of zinc oxide. *International Journal of Photoenergy*. **2016**.
- [38] Al-Hada, N. M.; Saion, E. B.; Shaari, A. H.; Kamarudin, M. A.; Flaifel, M. H.; Ahmad, S. H.; Gene, S. A. A facile thermal-treatment route to synthesize ZnO nanosheets and effect of calcination temperature. *PloS one*. **2014**, 9(8).

- [39] Baruah, S.; Dutta, J. pH-dependent growth of zinc oxide nanorods. *Journal of Crystal Growth*. **2009**, 311(8), 2549-2554.
- [40] Kumar, S. S.; Venkateswarlu, P.; Rao, V. R.; Rao, G. N. Synthesis, characterization and optical properties of zinc oxide nanoparticles. *International Nano Letters*. **2013**, 3(1), 30.
- [41] Wang, H.; Li, C.; Zhao, H.; Li, R.; Liu, J. Synthesis, characterization, and electrical conductivity of ZnO with different morphologies. *Powder Technology*. **2013**, 239, 266-271.
- [42] Rastogi, L.; Arunachalam, J. Sunlight based irradiation strategy for rapid green synthesis of highly stable silver nanoparticles using aqueous garlic (*Allium sativum*) extract and their antibacterial potential. *Materials Chemistry and Physics*. **2011**, 129(1-2), 558-563.
- [43] Rosi, N. L.; Mirkin, C. A. Nanostructures in biodiagnostics. *Chemical Reviews*. **2005**, 105(4), 1547-1562.
- [44] Sabir, S.; Arshad, M.; Chaudhari, S. K. Zinc oxide nanoparticles for revolutionizing agriculture: synthesis and applications. *The Scientific World Journal*. **2014**.
- [45] Sawai, J.; Shoji, S.; Igarashi, H.; Hashimoto, A.; Kokugan, T.; Shimizu, M.; Kojima, H. Hydrogen peroxide as an antibacterial factor in zinc oxide powder slurry. *Journal of Fermentation and Bioengineering*. **1998**, 86(5), 521-522.
- [46] Shah, A. H.; Manikandan, E.; Ahamed, M. B.; Mir, D. A.; Mir, S. A. Antibacterial and Blue shift investigations in sol-gel synthesized $\text{Cr}_x\text{Zn}_{1-x}\text{O}$ Nanostructures. *Journal of Luminescence*. **2014**, 145, 944-950.
- [47] Shanker, U.; Jassal, V.; Rani, M.; Kaith, B. S. Towards green synthesis of nanoparticles: from bio-assisted sources to benign solvents. A review. *International Journal of Environmental Analytical Chemistry*. **2016**, 96(9), 801-835.

- [48] Suntako, R. Effect of zinc oxide nanoparticles synthesized by a precipitation method on mechanical and morphological properties of the CR foam. *Bulletin of Materials Science*. **2015**, 38(4), 1033-1038.
- [49] Sinha, R.; Karan, R.; Sinha, A.; Khare, S. K. Interaction and nanotoxic effect of ZnO and Ag nanoparticles on mesophilic and halophilic bacterial cells. *Bioresource Technology*. **2011**, 102(2), 1516-1520.
- [50] Leroch, M.; Kretschmer, M.; Hahn, M. Fungicide resistance phenotypes of *Botrytis cinerea* isolates from commercial vineyards in South West Germany. *Journal of Phytopathology*. **2011**, 159(1), 63-65.
- [51] Li, Q.; Mahendra, S.; Lyon, D. Y.; Brunet, L.; Liga, M. V.; Li, D.; Alvarez, P. J. Antimicrobial nanomaterials for water disinfection and microbial control: potential applications and implications. *Water Research*. **2008**, 42(18), 4591-4602.
- [52] Lipovsky, A.; Nitzan, Y.; Gedanken, A.; Lubart, R. Antifungal activity of ZnO nanoparticles- the role of ROS mediated cell injury. *Nanotechnology*. **2011**, 22(10), 105101.
- [53] Padmavathy, N.; Vijayaraghavan, R. Enhanced bioactivity of ZnO nanoparticles- an antimicrobial study. *Science and Technology of Advanced Materials*. **2008**, 9(3), 035004.
- [54] Singh, P.; Kim, Y. J.; Zhang, D.; Yang, D. C. (2016). Biological synthesis of nanoparticles from plants and microorganisms. *Trends in Biotechnology*. **2016**, 34(7), 588-599.
- [55] Baruah, S.; Dutta, J. Hydrothermal growth of ZnO nanostructures. *Science and Technology of Advanced Materials*. **2009**, 10(1), 013001.
- [56] Wahab, R.; Ansari, S. G.; Kim, Y. S.; Seo, H. K.; Kim, G. S.; Khang, G.; Shin, H. S. Low temperature solution synthesis and characterization of ZnO nano-flowers. *Materials Research Bulletin*. **2007**, 42(9), 1640-1648.

- [57] Chen, C.; Liu, P.; Lu, C. Synthesis and characterization of nano-sized ZnO powders by direct precipitation method. *Chemical Engineering Journal*. **2008**, 144(3), 509-513.
- [58] Thirumavalavan, M.; Huang, K. L.; Lee, J. F. Preparation and morphology studies of nano zinc oxide obtained using native and modified chitosans. *Materials*. **2013**, 6(9), 4198-4212.
- [59] Shamhari, N. M.; Wee, B. S.; Chin, S. F.; Kok, K. Y. Synthesis and characterization of zinc oxide nanoparticles with small particle size distribution. *ActaChimicaSlovenica*. **2018**, 65(3), 578-585.